

PACS numbers: 52.38.Kd; 52.38.Mf; 52.38.Ph
DOI: 10.1070/QE2001v031n03ABEH001925

Generation of hot particles in a femtosecond laser-produced plasma with the use of solid modified targets

R V Volkov, S A Gavrilov, D M Golishnikov, V M Gordienko,
P M Mikheev, A B Savel'ev, A A Serov

Abstract. **Specific features of the interaction of ultrashort laser pulses with solid modified targets are considered. Our experimental studies show that the use of such targets increases the 'temperature' of hot plasma electrons. The spatial and temporal structure of the ion current of the plasma is investigated.**

Keywords: *femtosecond laser plasma, modified targets, hot electrons, X-ray emission, fast ions.*

1. Introduction

Investigations that have been performed so far show that many parameters of the plasmas produced on modified surfaces under the action of femtosecond laser pulses with an intensity exceeding 1 PW cm^{-2} considerably differ from the parameters of plasmas produced by the laser irradiation of flat surfaces [1–7]. Thus, the yields of soft and hard X-ray emission [1–4], the 'temperature' of hot electrons [4], the efficiency of second harmonic generation [5], etc. are increased at the same intensity of laser pulses. Target surfaces were structured in different ways: from the use of diffraction gratings (including gratings induced by a pair of femtosecond laser pulses interfering on the surface of a target [5]) to the formation of a thick porous layer on the surface of the sample ('black' gold deposition [1, 2] and electrochemical etching resulting in the formation of high-porosity silicon [3, 4, 6–8]).

This paper continues our studies earlier presented in [3–5, 7, 8]. We will consider the specific features of the interaction of ultrashort laser pulses with solid modified targets and experimentally investigate the generation of hot plasma electrons and hard X-ray emission in such targets.

R V Volkov International Education and Research Laser Centre, M V Lomonosov Moscow State University, Vorob'evy gory, 119899 Moscow, Russia
S A Gavrilov Moscow Institute of Electric Engineering, Zelenograd, 103498 Moscow, Russia
D M Golishnikov, V M Gordienko, P M Mikheev, A B Savel'ev Department of Physics, M V Lomonosov Moscow State University, Vorob'evy gory, 119899 Moscow, Russia
A A Serov Research Institute of Automation, Mospochtampt, P.O. Box 918, 101000 Moscow, Russia

Received 24 October 2000
Kvantovaya Elektronika **31** (3) 241–246 (2001)
Translated by A M Zheltikov

2. Specific features of the interaction of femtosecond laser pulses with nanostructured targets

The heating of electrons resulting from the interaction of ultrashort laser pulses with modified targets differs in several aspects from heating accompanying the interaction of radiation with plane solid targets. The initial absorption length of laser radiation can be estimated as [9]

$$l_0 \approx \frac{PV}{S}, \tag{1}$$

where $P = \rho_s/\rho_m$ is the ratio of the density of particles to the mean density of the modified layer (porosity); V and S are the volume and the cross section of particles, respectively. For spherical particles with a diameter of 5 nm and a layer porosity $P \sim 3-5$, the thickness l_0 is of the order of 15 nm. Fast heating of particles results in the formation of a plasma with a plasma frequency $\omega_p = [4\pi e^2 n_e/(m_e P)]^{1/2}$ (where m_e and n_e are the mass and the density of electrons). Laser radiation under these conditions is absorbed in a skin layer with a thickness equal to (in nanometers) [10]

$$l_s \approx \frac{c}{\omega_p}\left(\frac{\nu_{ei}}{\omega_0}\right)^{0.5} \approx 400\,\frac{Z^{1/2}\lambda^{1/2}}{T_e^{3/4}}, \tag{2}$$

where ν_{ei} is the frequency of electron–ion collisions; ω_0 is the frequency of laser radiation; Z is the degree of plasma ionisation; λ is the wavelength of laser radiation in microns; and T_e is the temperature of thermal plasma electrons in electronvolts. For typical values of these parameters ($Z \sim 10$ and $T_e \sim 500$ eV), the thickness of the skin layer is $l_s \sim 12$ nm, which corresponds to the initial length l_0.

The oscillation amplitude of a free electron (in nanometers) is [10]

$$L_e \approx 3I_{15}^{1/2}\lambda^2 \tag{3}$$

where I_{15} is the intensity of laser radiation in PW cm^{-2} and λ is the wavelength in microns. With an intensity of laser radiation $I > 10$ PW cm^{-2}, this amplitude is of the order of the characteristic size of a structural element in the surface layer of a target or exceeds this size (2–10 nm in high-porosity silicon and 100 nm for laser-modified samples). This implies that the role of collisionless absorption increases even for moderate intensities.

Structured targets are also characterised by the increase in the area of the surface interacting with a plasma and,

consequently, by the increase in the total number of hot plasma electrons. The energy of hot electrons is of the order of the electron quiver energy (in electronvolts) in an external electromagnetic field,

$$\varepsilon_{osc} \approx 90 I_{15} \lambda^2 \quad (4)$$

and is about 1 keV for an intensity of 10 PW cm^{-2}. These electrons play a key role in hard X-ray plasma emission. In addition, efficient resonant absorption, generation of plasma waves, and build-up of plasma instabilities allow further acceleration of electrons up to even higher energies [10].

The fact that the expansion of separate structure elements and pore erosion occur within time intervals comparable with the duration of a typical laser pulse ($\sim$ 100 fs) has a considerable influence on the character of interaction of laser radiation with a modified near-surface layer and parameters of the plasma produced under these conditions. The characteristic time of structure erosion (in femtoseconds) can be estimated from the energy conservation law as

$$t \approx \frac{L}{u} = 15L\left(\frac{n_i d}{2KI_{15}\tau PA}\right)^{1/2}, \quad (5)$$

where L is the distance between the structure elements in nanometers; u is the mean ablation rate of the target material; d is the thickness of the plasma layer in microns; n_i is the concentration of ions in 10^{22} cm^{-3}; A is the atomic number of the target material; τ is the duration of the laser pulse in hundreds of femtoseconds; and $K \sim 0.1 - 0.3$ is the coefficient of conversion of laser radiation energy into the ion expansion energy. With $L \sim 5 - 50$ m, $P \sim 5$, $d \sim 0.1$ μm, $n_i \sim 5$, $A \sim 30$, $\tau \sim 2$, and $I_{15} \sim 10$, we arrive at $t \sim 25$ – 250 fs.

In the process of formation of a homogeneous plasma with a lowered density, the kinetic energy of ions is transformed into the thermal energy of ions due to ion–ion collisions. The ion temperature T_i under these conditions becomes of the order of the ion kinetic energy, $E_a \approx m_i u^2/2$ (where m_i is the ion mass), and may reach tens of kiloelectronvolts. The high efficiency of this process can be achieved when two conditions are satisfied: the ion mean free path length L_i should be much less than the plasma size and the inverse frequency of ion–ion collisions $\nu_{ii}^{-1} = \tau_{ii}$ should be less than the electron–ion relaxation time τ_r and the characteristic time of plasma cooling τ_a. The time τ_{ii} (in femtoseconds) can be estimated from the formula

$$\tau_{ii} \approx 0.4 \frac{A^{1/2} E_a^{3/2} P}{Z^4 n_i}. \quad (6)$$

The following expression can be easily derived for the time τ_r (in picoseconds):

$$\tau_r = \nu_{ei}^{-1} \frac{m_i}{2m_e} \approx 6 \cdot 10^{-3} \frac{T_e^{3/2} AP}{Z^2 n_i}. \quad (7)$$

For the chosen plasma parameters, we have $\tau_{ii} \sim 1$ ps, $\tau_r \sim$ 10 ps, and the plasma cooling time τ_a always exceeds 10 ps [10].

The length L_i can be estimated from the following simple expression: $L_i = u\tau_{ii}$. Our estimates show that the ion mean free path length $L_i \approx 10 - 50$ nm is much less than the plasma thickness d. We should note that total plasma homogenisation does not occur instantaneously. Apparently, this process is accompanied by density oscillations, whose frequency is determined by the inverse time t of pore erosion and the decay time [11]

$$t_d \approx \frac{3L^2}{uL_i}, \quad (8)$$

which ranges from $\sim$ 25 fs up to $\sim$ 2.5 ps ($t_d \gg t$) as L increases from 5 to 50 nm. Such ion density oscillations may give rise to a modulation of the electron density, which, in its turn, may lead to the generation of plasma waves and electron acceleration.

Thus, in solid-density structured targets, the ion plasma component is heated up to a temperature of tens of kiloelectronvolts within time intervals comparable with the duration of a laser pulse. In a 'conventional' plasma, on the other hand, the ion temperature reached within time intervals shorter than 1 ps never exceeds 50 eV.

We should note that the analysis performed above is also partially applicable for colloidal metal targets [1, 2] and cluster targets [12]. However, the ion density n_i is low in these cases ($n_i \approx 10^{19} - 10^{20}$ cm^{-3}). Consequently, both the mean free path length and the inverse frequency of ion–ion collisions may become large. For parameters of experiments [1, 2], we have $d < L_i \sim 1$ μm and $t \sim \tau_{ii} \sim 3$ ps, while in the case of a cluster target [12], we find that $d \sim L_i \sim 100$ μm and $t \sim \tau_{ii} \sim 300$ ps. These estimates show that the conditions for the formation of a plasma with an anomalously high ion temperature are satisfied only partially in these cases.

3. Experimental

We used radiation of a femtosecond laser system [3], which generated pulses with a wavelength of 610 nm, duration of 200 fs, an energy up to 1 mJ, and a pulse repetition rate of 1 Hz. When a special aberration-free objective was used to focus a laser beam into a spot with a diameter of 3 μm, the radiation intensity on the target was as high as 50 PW cm^{-2}. The radiation intensity contrast under these conditions was higher than 10^5. Most of our experiments were carried out with p-polarised radiation (unless otherwise is mentioned in the text). A target was placed in a vacuum chamber with a residual gas pressure up to 10^{-5} Torr (see Fig. 1). The angle of incidence of laser radiation on the target was equal to 45°.

Plane polished single-crystal or high-porosity (with a porosity $P = 5 - 6$) silicon plates or a titanium film with a surface density of 2.5 mg cm^{-2} on a molybdenum substrate with a thickness of 300 μm were used as initial targets in our experiments. Laser modification of sample surfaces was performed with radiation of the above-described laser system directly in experiments devoted to the investigation of plasma properties. The first laser pulse in these experiments produced a crater, which served as a target for the next laser pulse.

Fig. 2a shows an SEM image of a crater on the surface of a titanium target. The angle between the normal to the target plane and an electron beam was equal to 30°. The crater diameter is $\sim$ 10 μm, while the crater depth is estimated as 1–2 μm. A submicron structure arising inside the crater can is clearly seen in this image. We should note that a

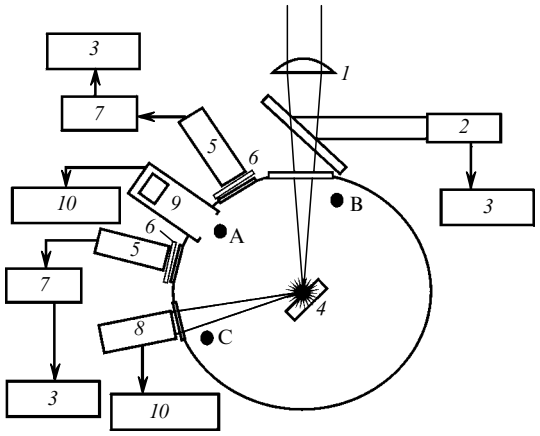

Figure 1. Experimental setup: (*1*) focusing objective, (*2*) pyroelectric detector of laser radiation energies, (*3*) multichannel analogue-to-digital converter, (*4*) target, (*5*) X-ray detectors, (*6*) X-ray filters, (*7*) charge-sensitive amplifiers, (*8*) photoelectric cathode, (*9*) time-of-flight ion detector, and (*10*) fast multichannel analogue-to-digital converter; A, B, and C indicate three possible positions of the detector *9*.

similar image was obtained in [13], where an iron target was irradiated with a low-contrast femtosecond pulse. However, no crater was produced under conditions of experiments [13], and submicron structures were formed on the surface of the target. Repeated irradiation of a crater increases the crater depth, resulting in a gradual formation of a hole, which grows toward the inside of the target at the angle corresponding to the incidence angle of laser radiation on the target (see Fig. 2b). Subsequent measurements have shown that the yield of hard X-ray emission from the target starts to lower after 4–5 shots per one spot on the surface and completely vanishes after 6–7 shots.

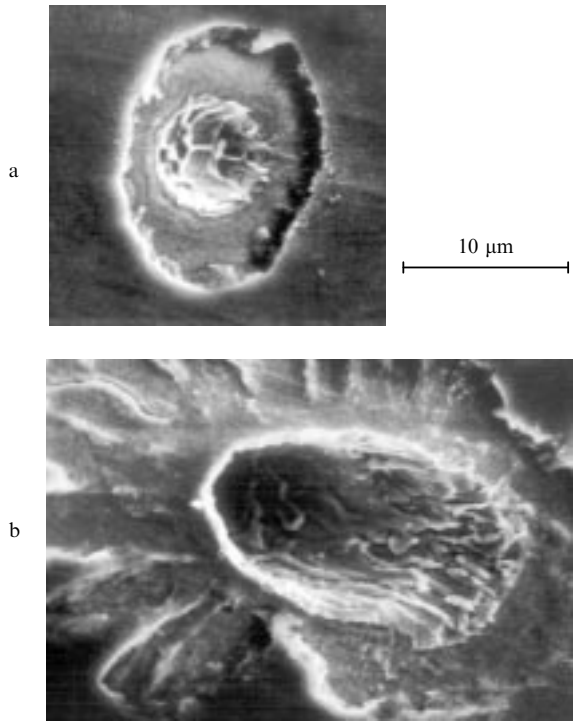

Figure 2. Electron-microscope images of craters on the surface of a titanium target produced with (a) single and (b) multiple irradiation of the target. The angle of incidence of the electron beam is 30°.

A two-channel detector of hard X-ray emission from the plasma (for estimating the 'temperature' of hot plasma electrons in each laser pulse [14]) and a time-of-flight ion spectrometer were used in our experiments for plasma diagnostics (see Fig. 1).

The spatial distribution of the ion current was investigated for three different experimental geometries: the spectrometer was placed either along the normal to the surface of the target (position A) or at an angle of 70° with respect to the normal from the side of the incident (position B) or reflected (position C) laser beam. A VEU-9 unit with a chevron microchannel plate placed at a distance of 22 cm from the target was used to detect and amplify the ion current. For calibrating the zero point of the time scale, the light signal reflected from the plasma was detected with a photoelectric cathode and was entered into an analogue-to-digital converter, which ensured the timing of plasma excitation with an accuracy higher than 10 ns.

4. Experimental results

The yield X of hard X-ray emission from different targets as a function of the intensity I of laser radiation was studied within spectral ranges with a lower boundary from 5 up to 100 keV using a set of beryllium, aluminium, and tantalum foils with different thicknesses [14]. Within all the studied spectral ranges, the yield X increased with the growth in I for high-porosity (HP) and laser-modified (LM) targets faster than in the case of a solid plane target. When the yield X is approximated with an exponential function CI^{α}, the shift of the transmission band of filters toward higher energies E of X-ray quanta results in a gradual increase in the exponent α from ~ 2 ($E > 4$ keV) up to ~ 4 ($E > 15$ keV, see the details in [8]. The increase in the temperature of hot electrons in modified targets is seen most clearly within the ranges of quantum energies $E > 35$ keV (see Fig. 3). No signal was observed for a standard plane silicon target, while HP and LM targets produced a stable signal corresponding to the detection of X-ray quanta with energies of 35–100 keV.

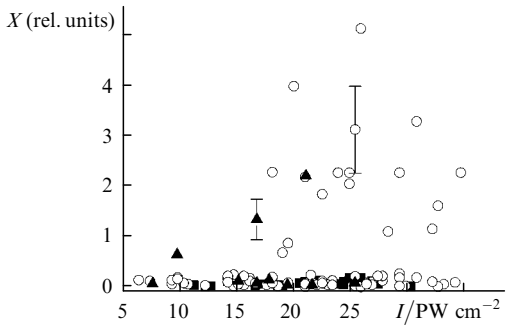

Figure 3. The yield X of hard X-ray emission with the energy of quanta higher than 35 keV as a function of the intensity I of laser radiation for crystalline silicon under (■) single and (○) multiple laser irradiation and (▲) for porous silicon under multiple irradiation.

Fig. 4 presents a histogram of temperature distribution for the hot electron component in the case of crystalline silicon and LM silicon irradiated with 20 ± 10 PW cm^{-2}

laser pulses. The width of this distribution reflects fluctuations of duration and energy of laser pulses. Much larger fluctuations observed in the case of LM silicon are apparently due to the instability of parameters of the laser-produced structure. The estimate for the mean 'temperature' of hot electrons in the case of crystalline silicon, $T_h \sim 5.2 \pm 1$ keV, agrees well with the available experimental data and theoretical calculations [10]. A similar estimate for LM silicon gives $T_h \sim 8.4 \pm 2$ keV, indicating the overheating of the hot electron component in LM silicon.

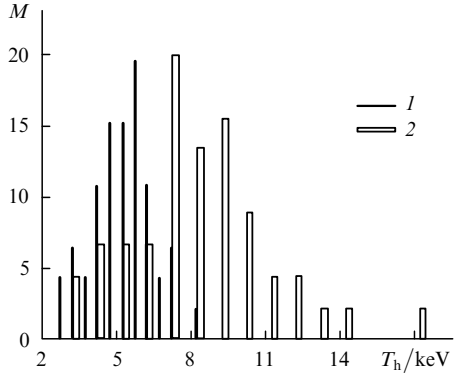

Figure 4. The histogram showing the distribution of the number M of realisations with a given 'temperature' of hot electrons over the 'temperature' T_h for a silicon target under (*1*) single and (*2*) multiple laser irradiation.

Our experimental data allow us to estimate the change in the 'temperature' of hot electrons as a function of laser intensity (Fig. 5). Approximation of the experimental data for crystalline silicon yields (in kiloelectronvolts) $T_h \approx 3.3 I_{16}^{0.63}$ (the intensity is normalised to 10 PW cm^{-2}). The exponent $\alpha = 0.63$ corresponds to the regime of anomalous skin effect [10]. For an HP target, the exponent increases up to 1.4. In the case of an LM silicon target, a considerable scatter of experimental data does not allow us to find a reliable approximation. However, the mean 'temperature' of the hot electron component is even higher than in the case of HP silicon. The results of these experiments provide a convincing evidence of the growing role of collisionless absorption in structured solid targets. Obviously, this effect requires a further theoretical analysis.

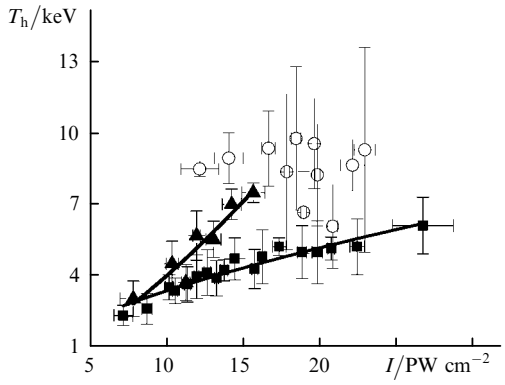

Figure 5. The 'temperature' T_h of hot electrons as a function of the laser radiation intensity I (see the notation in Fig. 3).

The detected growth in the 'temperature' of the hot electron component is manifested also in time-of-flight spectrometric measurements of the current related to the ion plasma component. First, we will consider the results obtained in the case when the detector was placed along the normal to the target in position A (Fig. 1). Two components can be seen in Fig. 6a in this case: a fast component with a velocity up to $u_f \sim 2 \times 10^8$ cm s^{-1} and a slow component with a velocity lower than 10^8 cm s^{-1}. The mean velocity of the slow component is approximately equal to the mean velocity u of target material expansion ($u \sim 4 \times 10^7$ cm s^{-1} for our experimental conditions). The velocity corresponding to the maximum of the fast component increases with the growth in the intensity as $I^{0.2 \pm 0.03}$, which is consistent with the results of [15], obtained for laser intensities exceeding 100 PW cm^{-2}.

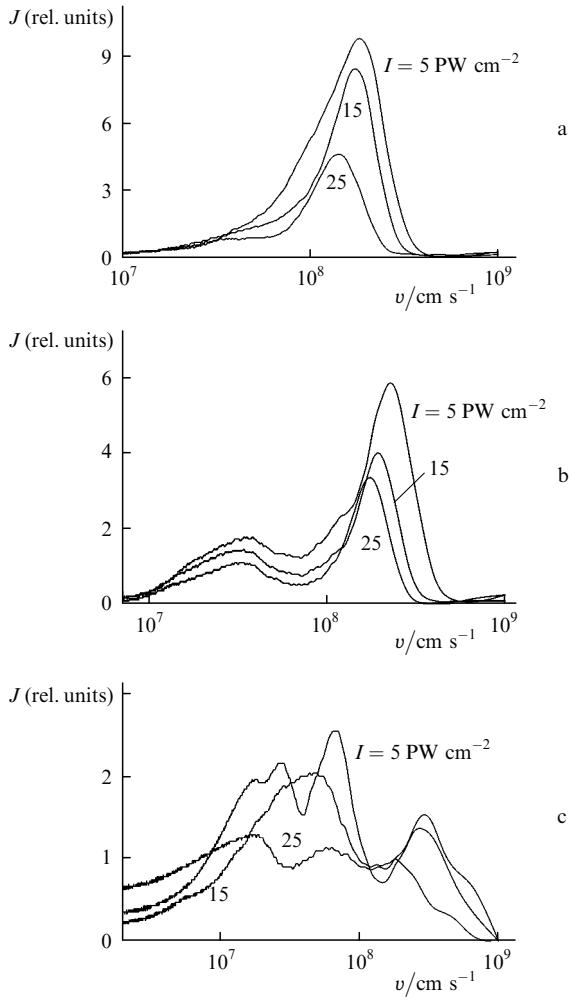

Figure 6. The amplitude of the ion current J as a function of the expansion velocity of ions v for a detector in the position A (see Fig. 1) under conditions of (a) single and (c) multiple laser irradiation of crystalline silicon and (b) under conditions of single laser irradiation of porous silicon for different laser intensities.

Similar dependences (but with lower expansion velocities) were observed in [16] for lower laser radiation intensities. Since the velocity of ion expansion in a plasma is proportional to the electron temperature, $v_{e,h} \sim T_{e,h}^{1/2}$, ion measurements confirm the existence of two electron com-

ponents in the plasma under study: a thermal component with a temperature T_e and a hot component with a 'temperature' T_h. Similar observations were earlier reported in [16, 17]. We should note that, when an s-polarised radiation is used in experiments, the amplitude of the ion signal drastically decreases and the maximum of the signal corresponding to the hot electron component vanishes. These effects are due to the low efficiency of generation of hot electrons with such a polarisation of the laser field [10].

Analogous dependences were also observed for an HP target (Fig. 6b). The main differences of these dependences from the case of a plane target with approximately the same laser intensities are associated with a more clearly pronounced thermal component (with the velocity corresponding to the maximum of the ion current equal to 3×10^7 cm s^{-1}) and a higher (by 20 – 30 %) velocity of the hot component. A considerable fraction of energy absorbed by laser-heated clusters in HP silicon is transformed, in contrast to the plane expansion of a crystalline target, into the energy of volume expansion of clusters. Due to the collisions of ion jets, this energy is transformed into the thermal energy of ions. The gas-kinetic plasma pressure $p = n_i(ZT_e + T_i)$ remains virtually unchanged under these conditions, while the relative fraction of ions ejected from the plasma with a thermal velocity increases. This explains the redistribution of the amplitudes of slow and fast ion components in Fig. 6b.

Radically different dependences, featuring several (up to 4 – 5) maxima, are observed in the case of an LM target (Fig. 6c). Positions of maxima vary in this case from realisation to realisation. At the same time, the maximum corresponding to the fast ion component is observed quite robustly. The propagation velocity of this component, $u_f \sim (2 - 3) \times 10^8$ cm s^{-1}, exceeds the propagation velocity u_f attainable with targets of other types. The appearance of several maxima corresponding to lower velocities may be due to a substantial spatial inhomogeneity of the arising ion flow caused by the inhomogeneity of the initial target crater. Indeed, the time of structure erosion for the employed HP target ($P \sim 5$) is $t \sim 100$ fs. This results in an efficient homogenisation of the ion plasma component before plasma expansion into the vacuum. For an LM target, the porosity P, estimated from the data obtained by means of electron and atomic-force microscopy, is also ~ 5. However, the time t is greater in this case ($t \sim 25$ ps) due to larger geometric sizes of the voids: $L \sim 0.3 - 1$ μm. This may imply no efficient homogenisation of the ion plasma component in the case of an LM target, thus explaining the nonstationary turbulent plasma expansion into the vacuum observed in experiments.

Another important finding is that the polarisation of laser radiation has no influence on the ion current. Specifically, when the polarisation is rotated by 90°, the waveform of the ion current and the characteristic velocities of ion propagation remain unchanged. This is obviously related to the curvature and the large-scale inhomogeneity of the crater surface.

Considerable changes in the ion current were observed when the time-of-flight spectrometer was placed on the side of either incident or reflected laser radiation (positions B and C, Fig. 7). Only the slow component of the ion current is detected in this case for both crystalline and porous targets. No noticeable differences in the ion current were observed for these two positions of the detector. These results indicate that the hot ion component propagates in the form of a cone along the normal to the average target surface. Ion currents detected in the case of an LM target reveal the presence of a fast ion component (whose propagation velocity is somewhat lower than the velocity of propagation along the normal to the target). An unstable multipeak structure was observed in this case, and no dependence on the polarisation of laser radiation was noticed.

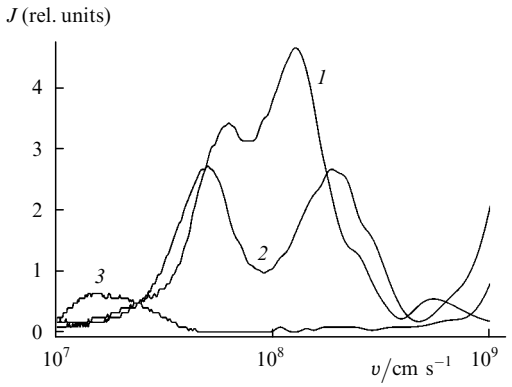

Figure 7. The amplitude of the ion current J as a function of the expansion velocity of ions v for a detector in the position B or C (see Fig. 1) under conditions of multiple laser irradiation of silicon with laser intensities (*1*) $I = 20$ and (*2*) 25 PW cm^{-2} and (*3*) single laser irradiation of silicon with $I = 20$ PW cm^{-2}.

5. Conclusions

Our studies have shown that, along with various methods of preparing targets with structured near-surface layers employed earlier (deposition in a rare-gas atmosphere and electrochemical etching of silicon), laser modification of a target surface also ensures the formation of a structured layer directly in the process of experiments.

The 'temperature' of the hot electron component in the case of modified targets increases with the growth in laser intensity faster than in the case of a continuous target, reaching 8 – 10 keV for a laser intensity of 20 PW cm^{-2}. This effect leads to the shifting of the spectrum of X-ray plasma emission toward shorter wavelengths. At the same time, the experimentally observed generation of X-ray quanta with energies of 40 – 100 keV cannot be explained by the growth in the 'temperature' of the hot electron component up to 8 keV (relative to the X-ray yield in other energy ranges). This indicates the appearance of a substantially non-Maxwellian tail of the electron distribution in the plasma, making the notion of 'temperature' rather arbitrary for the hot electron component.

The ion plasma component is subject to considerable changes in modified targets. On the other hand, the growth in the 'temperature' of the hot electron component increases the expansion velocity of some part of ions up to $(2-3)\times10^8$ cm s^{-1} and gives rise to energies of silicon ions above 100 keV. The energy of this ion component increases with the intensity growth as $I^{0.4}$. On the other hand, the mixing of ion jets inside the plasma steeply increases the ion plasma temperature from 30 – 50 eV up to several and even tens of kiloelectronvolts. This effect becomes possible due to a high plasma density in the case of modified targets, since the

frequency of ion–ion collisions for densities of the order of the critical density (which is characteristic of the targets of the cluster-jet type) is low compared to the inverse time of ablation lowering of the plasma density. For LM targets, we observed a nearly isotropic plasma expansion into the vacuum. Such a behaviour was characteristic of both thermal and hot ion components.

Thus, plasma formation in modified solid targets irradiated with laser pulses with moderate intensities of $10-100$ PW cm^{-2} may be accompanied by the increase in the 'temperature' of hot electrons and the growth in the number of such electrons. A strongly nonequilibrium plasma with an ion temperature of $1-50$ keV may arise under these conditions. This opens an opportunity of performing several unique experiments, including experiments on nuclear processes in a femtosecond laser-produced plasma. Until now, the realisation of such experiments was related to the use of large laser systems generating relativistic laser intensities. In fact, we are discussing nuclear processes occurring within a small volume with a low energy deposition in a target. This fact was confirmed by our experiments on initiating a thermonuclear reaction in the plasma of a deuterated LM target [18].

Acknowledgements. This study was supported by the Russian Foundation for Basic Research (Grant No. 99-02-18343a) and the 'Fundamental Metrology' and the 'Universities of Russia' Science and Technology Federal Programs.

References

1. Murnane M M, Kapteyn H C, Gordon S P, et al. *Appl. Phys. Lett.* **62** 1068 (1993); *Appl. Phys B* **58** 261 (1994)
2. Wulker C, Theobald W, Gnass D R, et al. *Appl. Phys. Lett.* **68** 1338 (1996)
3. Volkov R V, Gordienko V M, Dzhidzhoev M S, et al. *Kvantovaya Elektron.* **24** 1114 (1997) [*Quantum Electron.* **27** 1081 (1997)]
4. Volkov R V, Gordienko V M, Dzhidzhoev M S, et al. *Kvantovaya Elektron.* **25** 1 (1998) [*Quantum Electron.* **28** 3 (1998)]
5. Volkov R V, Gordienko V M, Dzhidzhoev M S, et al. *Kvantovaya Elektron.* **23** 539 (1996) [*Quantum Electron.* **26** 524 (1996)]
6. Nishikawa T, Nakano H, Ahn H, et al. *Appl. Phys. Lett.* **70** 1653 (1997); *Appl. Phys. B* **66** 567 (1998)
7. Gordienko V M, Savel'ev A B *Usp. Fiz. Nauk* **167** 78 (1999) [*Phys. Usp.* **169** 72 (1999)]
8. Gavrilov S A, Golishnikov D M, Gordienko V M, et al. *Proc. SPIE* **4070** 206 (2000)
9. Gus'kov S Yu, Rozanov V B *Kvantovaya Elektron.* **24** 715 (1997) [*Quantum Electron.* **27** 696 (1997)]
10. Gibbon P., Foster E. *Plasma Phys. Control. Fusion* **38** 769 (1996)
11. Gus'kov S Yu, Caruso A, Rozanov V B, Strangio K *Kvantovaya Elektron.* **30** 191 (2000) [*Quantum Electron.* **30** 191 (2000)]
12. Ditmire T, Donelly T, Rubenchik A M, et al. *Phys. Rev. A* **53** 3379 (1996)
13. Stuart B C, Feit M D, Herman S, et al. *J. Opt. Soc. Am. B* **13** 458 (1996)
14. Volkov R V, Gordienko V M, Mikheev P M, Savel'ev A B *Kvantovaya Elektron.* **30** 896 (2000) [*Quantum Electron.* **30** 896 (2000)]
15. Clark E L, Krushelnik K, Zepf M, et al. *Phys. Rev. Lett.* **85** 1654 (2000)
16. Meyerhofer D D, Chen H, Delettrez J A, et al. *Phys. Fluids B* **5** 2585 (1993)
17. Andreev A A, Bayanov V I, Van'kov A B et al. *Kvantovaya Elektron.* **23** 907 (1996) [*Quantum Electron.* **26** 884 (1996)]
18. Volkov R V, Golishnikov D M, Gordienko V M, et al. *Pis'ma Zh. Eksp. Teor. Fiz.* **72** 577 (2000)